

Study of Citric Acid-Locust Bean Gum as a Glidant to Fillers of Cellulose Derivatives

Wuryanto Hadinugroho^{1*}

¹Faculty of Pharmacy, Widya Mandala Surabaya Catholic University, Surabaya, 60112, Indonesia

*Corresponding author: wuryanto.hadinugroho@gmail.com

Abstract

Citric acid-locust bean gum (CA-LBG) was introduced as an excipient in tablet preparations. CA-LBG is a compound derived from the esterification of citric acid (CA) with locust bean gum (LBG). The experiment aimed to determine the potential and effect of CA-LBG as a glidant on microcrystalline cellulose (MCC). The CA-LBG concentrations in the experiments were 0.5%, 1.0%, 2.0%, and 4.0%. Talc and magnesium stearate (MgS) as a comparison. The mixtures were evaluated for flow rate and angle of repose. The mixture was compressed into tablets weighing 700 mg. Tablets were evaluated for weight, hardness, and friability. The flow rate of the mixture containing CA-LBG 0.5%-4.0% was 12.77 g.sec⁻¹-15.96 g.sec⁻¹. The angle of repose of the mixture containing CA-LBG 0.5%-4.0% is 32.62°-35.52°. The weight of tablets containing CA-LBG 0.5%-4.0% is 700.0 mg-701.2 mg. The hardness of tablets containing CA-LBG 0.5%-4.0% is 6.30 kp-6.90 kp. The friability of tablets containing CA-LBG 0.5%-4.0% is 0.17%-0.36%. The CA-LBG has the potential as a glidant in MCC fillers. Increasing CA-LBG concentration causes the flow rate to increase, the angle of repose to decrease, and the hardness to increase. CA-LBG concentrations of 0.5% and 4.0% reduced tablet friability.

Keywords

Citric Acid-Locust Bean Gum, Citric Acid, Esterification, Glidant, Locust Bean Gum

Received: 8 November 2023, Accepted: 11 May 2024

<https://doi.org/10.26554/sti.2024.9.3.613-620>

1. INTRODUCTION

Citric acid-locust bean gum (CA-LBG) was introduced as an excipient in tablet preparations. The published uses of CA-LBG are as a tablet disintegration agent and negative matrix in controlled-release tablets (Hadinugroho et al., 2023, 2022a). CA-LBG is an ester material derived from the esterification of citric acid (CA) with locust bean gum (LBG) under acidic conditions. CA-LBG has been characterized by carbonyl ester group, solubility, viscosity, esterified CA, glass transition temperature, crystallinity index, and particle morphology. CA-LBG particles have a non-polar and hydrophobic tendency, so CA-LBG has low solubility in water (Hadinugroho et al., 2017, 2019). CA-LBG is irregular in shape and has a wavy surface (Hadinugroho et al., 2019, 2023, 2022b). This character can act as a glidant in tablet formulation.

Glidant is a material that can interact with filler particles to improve flow properties. Glidant particles will be on the surface of the filler particles to cover porosity and smooth the surface of the filler particles. Changing the surface of the filler particles improves the movement of each particle (Awad et al., 2020). Glidant materials often used in pharmaceutical preparation formulations are talc and magnesium stearate (MgS). Talc and MgS particles are fine powders, hydrophobic, insoluble in water, irregular in shape and platy wavy (Meng et al., 2022;

Pratiwi et al., 2017; Sheskey et al., 2017; Zarmpi et al., 2020). The character of CA-LBG particles is similar to that of talc and MgS particles, thus indicating that CA-LBG is capable of glidant.

The experiments aimed to determine the potential and influence of CA-LBG as a glidant in tablet formulation. The experiment used microcrystalline cellulose (MCC), commonly used as a filler in tablet formulations. MCC particles experience plastic deformation after compression, resulting in varying porosity in the tablet (Krivokapić et al., 2020). The experiment used CA-LBG with concentrations of 0.5%, 1.0%, 2.0%, and 4.0%. Talc and magnesium stearate were used as a comparison with the same concentration. Each mixture was evaluated for flow rate and angle of repose. The mixture is then compressed directly into tablets 700 mg. Tablets were evaluated for weight, hardness, and friability. MCC was chosen as the filler model in this experiment because MCC is a filler that is often used in tablets using the direct compression method. MCC particles are water-insoluble, irregularly oval, porosity, and hydrophobic (Pratiwi et al., 2017; Sheskey et al., 2017).

The novelty of this experiment is using CA-LBG as a glidant in MCC tablet filler to observe its potency and effect at various concentrations. This experiment explores the function of CA-LBG as a glidant for tablet formulation. In the fine

form of CA-LBG, the shape of the CA-LBG particles is irregular, has a wavy surface, is difficult to dissolve in water, and is hydrophobic (Hadinugroho et al., 2019, 2023, 2022a). In addition, the experiment's success provides a choice of future glidant in pharmaceutical excipients.

2. EXPERIMENTAL SECTION

2.1 Materials

The materials are locust bean gum ($C_{32}H_{56}O_{26}$) (food grade) (Viscogum, Cargill, France), citric acid monohydrate ($C_6H_8O_7 \cdot H_2O$) (pro analysis) (Merk KgaA, Darmstadt, Germany), hydrochloric acid (HCl) (pro analysis) (Sigma Aldrich Chemie, GmbH, USA), water for injection (H_2O) (sterile water) (PT. Ot-suka Indonesia), distilled water (H_2O) (technical grade) (Cawan Anugerah Chemika, Indonesia), acetone (C_3H_6O) (technical grade) (Cawan Anugerah Chemika, Indonesia), microcrystalline cellulose ($C_{14}H_{26}O_{11}$) (pharmaceutical grade) (Flocel PH 102, Gujarat Microwax Ltd, Gujarat, India), talc ($Mg_3Si_4O_{10}(OH)_2$) (food grade) (PT. Bratachem, Indonesia) and magnesium stearate ($C_{36}H_{70}MgO_4$) (food grade) (PT. Bratachem, Indonesia).

2.2 Methods

2.2.1 Synthesis of CA-LBG

The experiment used CA-LBG synthesized using methods adopted from previous research (Hadinugroho et al., 2022a). The manufacturing principle is that a certain amount of LBG (7.10×10^{-6} mol in 50 mL) that has been swollen is added to a certain amount of CA (0.42 mol) and HCl (0.24 mol) as a catalyst. The homogeneous mixture was UV irradiated. The mixture was then settled and washed repeatedly with acetone-distilled water. The CA-LBG precipitate was dried at room temperature ($\pm 25^\circ C$ for 72 hours) and powdered using a blender (Maspion, speed scale 4 for 8×5 minutes). Before being used in experiments, CA-LBG powder was characterized, including Fourier transform infrared (FTIR), nuclear magnetic resonance (NMR), X-ray (XRD), scanning electron microscope (SEM), viscosity, and pH.

2.2.2 Characterization of CA-LBG

A qualitative examination of chemical groups from CA-LBG infrared at $400-4000\text{ cm}^{-1}$ using UATR (Perkin Elmer Spectrum Version 10.4.3., USA). 1H and ^{13}C examination of CA-LBG using liquid state NMR spectrophotometer (JEOL RESONANCE ECZ 500R, 500 MHz, Japan). The CA-LBG diffractogram was recorded using X-ray of Cu; 1.54060Å; speed $4^\circ/\text{minute}$; slit . DS: 1° , SS: 1° , RS: 0.30 mm, and range $3.0200^\circ-80.0000^\circ (2\theta)$ (Lab X XRD 6000, Shimadzu, Japan). The CA-LBG particle surface was recorded at a distance of 10 mm voltage of 10 kV (SEM JSM-6510LA, JEOL, Japan). Viscosity examination of CA-LBG on spindle No. S61, 60 rpm, and torque $<10\%$ using a Brookfield viscometer (LVDV-I Prime, AP6510416, USA). The acidity examination of CA-LBG, CA, and LBG in solution (1% w/v) used a pH meter

calibrated to pH 4.0; 7.0; and 10.0 (Metrohm 913, Switzerland).

2.2.3 Preparation of a Mixture of MCC and Glidant

Each glidant (talc, MgS, and CA-LBG) was weighed according to the concentration of each experiment (Table 1). A quantity of MCC (Avicel PH 102) was weighed to complete up to 100 g. For one minute, glidant and MCC were mixed in a cubic mixer (Erweka, Germany). Each mixture was evaluated for flow rate and angle of repose. The mixture was compressed (Single punch, Erweka EP-1, Germany) into tablets weighing 700 mg, diameter ± 15 mm, hardness 5-12 kp (equivalent to compression force ± 2 tons). Tablets were evaluated for weight, hardness, and friability.

2.2.4 Flow Rate and Angel of Repose

The mixture (100 g) of glidant and MCC was poured into a flowability tester (Erweka, Germany). The equipment is pressed to start when the bottom valve of the funnel opens, and the mixture flows freely over the plate, forming a cone. The flow time is read on the monitor. The flow rate is obtained from the flow time ratio to the mixed powder's weight. The equipment then emits infrared light to measure the diameter and height of the cone. The angle of rest is read on the monitor (Aulton and Taylor, 2017; Hadinugroho et al., 2022a).

2.3 Weight

A total of 20 tablets were randomly selected and weighed one by one (Hadinugroho et al., 2022b). All weights obtained are averaged, and the standard deviation is determined.

2.4 Hardness

A total of 6 tablets were randomly selected and placed on a holder tester (Hadinugroho et al., 2022a; The United States Pharmacopeial Convention, 2018). The hard block presses the tablet until the tablet starts to fracture. The tablet hardness value is displayed on the monitor.

2.5 Friability

Tablets were randomly selected and dusted to weigh the equivalent of 6500 mg on an analytical balance (Hadinugroho et al., 2022a; The United States Pharmacopeial Convention, 2018). All tablets were placed in a friability tester apparatus tube. The tube was rotated at 25 rpm for 4 minutes. Once the rotation stops, each tablet is dusted again. Friability is the ratio of the difference between the treatment's initial and final weight to the initial weight.

2.6 Two-factor ANOVA

Apart from graphical analysis, the experiment was analyzed using a two-factor ANOVA for each parameter value. The factors used in ANOVA are the type of glidant and the experimental concentration. The parameters analyzed are flow rate, angle of repose, hardness, and friability (Hadinugroho et al., 2022a; The United States Pharmacopeial Convention, 2018). Analysis using the alpha (α) value is 0.05.

Table 1. Test Results on Mixtures and Tablets for Flow Rate, Angle of Repose, Weight, Hardness and Friability

Glidant	Concentration [%]	Test Code	Flow Rate [g.sec. ⁻¹]	Angle of Repose [°]	Weight [mg]	Hardness [kp]	Friability [%]
Talc	0.5	T0	9.29 ± 0.13	39.40 ± 0.14	702.2 ± 1.67	7.10 ± 0.38	0.15 ± 0.01
	1.0	T1	9.90 ± 0.20	38.64 ± 0.25	701.1 ± 1.43	7.20 ± 0.21	0.07 ± 0.02
	2.0	T2	10.31 ± 0.21	35.50 ± 0.19	700.2 ± 1.51	6.20 ± 0.22	0.13 ± 0.02
	4.0	T4	11.03 ± 0.19	34.75 ± 0.27	702.5 ± 1.69	6.00 ± 0.37	0.18 ± 0.03
MgS	0.5	M0	13.22 ± 0.10	37.50 ± 0.25	703.1 ± 1.47	7.10 ± 0.38	0.07 ± 0.02
	1.0	M1	13.70 ± 0.19	36.57 ± 0.10	702.6 ± 1.98	6.90 ± 0.22	0.14 ± 0.02
	2.0	M2	14.78 ± 0.34	34.49 ± 0.31	702.7 ± 1.53	6.60 ± 0.30	0.22 ± 0.03
	4.0	M4	13.46 ± 0.27	35.58 ± 0.24	702.4 ± 0.96	5.90 ± 0.31	0.37 ± 0.02
CA-LBG	0.5	C0	12.77 ± 0.25	35.52 ± 0.35	700.7 ± 1.87	6.30 ± 0.33	0.17 ± 0.02
	1.0	C1	13.33 ± 0.18	34.61 ± 0.18	701.2 ± 1.59	6.50 ± 0.47	0.28 ± 0.02
	2.0	C2	14.63 ± 0.12	33.49 ± 0.34	700.0 ± 1.37	6.60 ± 0.31	0.36 ± 0.02
	4.0	C4	15.96 ± 0.15	32.62 ± 0.33	702.1 ± 1.27	6.90 ± 0.27	0.23 ± 0.02

3. RESULTS AND DISCUSSIONS

3.1 Synthesis of CA-LBG

The synthesis for CA-LBG is divided into 30 batches because the synthesis is adjusted to lab scale capacity and facilities. The synthesis process followed fixed procedures in previous research by Hadinugroho et al. (2022b). Dry CA-LBG yield of all batches is 1.10 g ± 1.24 g. The CA-LBG all batches were homogenized and pureed using a blender (Maspion, speed scale 4 for 8 × 5 minutes). CA-LBG fines powder was used for characterization and experiments as a glidant.

3.2 Characterization of CA-LBG

The FTIR spectra of CA-LBG are presented in Figure 1. The infrared spectrum shows that the wave number of the O–H group appears at 3318.20 cm⁻¹; C–H appears at 2923.66 cm⁻¹ and 2851.10 cm⁻¹; and C=O ester appears at 1736.02 cm⁻¹. The NMR spectrum of CA-LBG are presented in Figure 2. Image ¹H CA-LBG NMR shows doublet peaks (2 pairs) at δ=2.927 ppm and δ=2.896 ppm; δ=2.744 ppm and δ=2.713 ppm, which correspond to C–H₂ of CA. Both peaks originate from symmetric C protons in CA. These peaks indicate the presence of CA in LBG. One adjacent proton causes a twist of the bond and a signal rupture. Multiplet peaks of mannose and galactose appeared at δ=3.990–3.329 ppm. Previous research reported that the two CA double peaks were around δ=3.083–2.714 ppm (Hadinugroho et al., 2022b, 2023). The peaks of two monomers of LBG appear between δ = 4.418–3.309 ppm (Hadinugroho et al., 2022b, 2023). The CA-LBG peaks in the ¹³C NMR examination were δ = 176.838 ppm; δ=173.449 ppm; δ = 173.363 ppm; δ = 100.154 ppm; δ = 98.762 ppm; 96.458 ppm; 76.550 ppm; δ = 75.034 ppm; δ = 73.316 ppm; 71.425 ppm; 69.946 ppm; 69.303 ppm; 60.981 ppm; 60.521 ppm; and 43.339 ppm. The peak δ=180–170 ppm corresponds to the C=O group. The peak δ=80–70 ppm corresponds to the central C atom. The peak δ=44–43 ppm corresponding to C–H and C–H₂ (Duan et al., 2020; Hadinu-

groho et al., 2019; Kim et al., 2017; Zhang et al., 2016). The peak δ=105–60 ppm corresponds to two monomers of LBG appearing at δ=105–60 ppm (Gillet et al., 2014; Hadinugroho et al., 2022b; Idström et al., 2016; Tian et al., 2023; Trabelsi et al., 2021). The diffractogram profile (Figure 3) shows that CA-LBG is an amorphous compound with a peak at 16.600 degrees, where this character is similar to previous research (Hadinugroho et al., 2019; Isasi and Ramón, 2022; Singh et al., 2020). The amorphous character of CA-LBG is dominated by the LBG character, which is a galactomannan polymer with an irregular molecular arrangement (Tikhonov et al., 2019; Zheng et al., 2022). The shape of CA-LBG particles (Figure 4) is like irregular coral with a wavy surface. There are sheets attached to the coral to confirm the presence of CA in LBG (Hadinugroho et al., 2017, 2022b). The CA-LBG test results for viscosity were 9.49 cP ± 0.08. This viscosity is close to previous research results of around 7.82–11.37 cP (Hadinugroho et al., 2019, 2023, 2022b). The CA-LBG test result for pH was 4.83. This result was compared with a CA pH of 2.05 and an LBG pH of 5.85. Tests were carried out on 1% w/v solutions of CA-LBG, CA, and LBG by dipping the pH meter electrode (Metrohm 913, Switzerland), which had been previously calibrated. The pH value of 4.83 proves that the presence of CA in LBG results in a pH value between the pH values of CA and LBG (1% b/v, pH ± 5.3) (Sheskey et al., 2017). The results of CA-LBG characterization using FTIR, NMR, XRD, SEM, viscosity, and pH show that the CA-LBG used is similar to previous experiments and can be used for further experiments as a glidant in MCC filler.

3.3 Flow Rate

The flow rate test results for all experiments are presented in Table 1 and Figure 5. In general, the mixture containing MgS (M0-M4) and CA-LBG (C0-C4) has a faster flow rate than the mixture containing talc. A good pharmaceutical flow rate for powder or powder mixture is ≥ 10 g.second⁻¹ (Fitrya

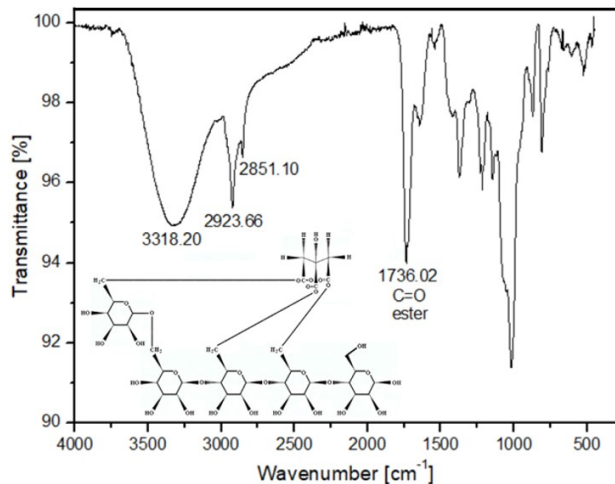


Figure 1. Infrared Spectra of CA-LBG

and A, 2021; Gustaman et al., 2021; Jayani et al., 2021; Luh Putu Wrasiasi and Putra, 2021; Putri, 2023; Zebua et al., 2023). MgS and CA-LBG particles can interact well on the surface of the MCC particles so that the two glidants can make it easier for them to flow. The mixture of each glidant showed a different flow rate profile. The mixture containing talc and CA-LBG showed that increasing the glidant concentration increased the flow rate of the mixture. The surface area of the MCC particles in the powder is sufficient to interact with many particles of talc and CA-LBG. The flow rate graphic of the mixture containing MgS (M0-M2) was initially similar to the flow rate graphic of the other two glidants, but at an MgS concentration of 4% (M4), the flow rate decreased. The number of MgS particles (M4) exceeds the number of MCC particles, so the surface area of the MCC particles in the powder is insufficient to interact with the MgS particles, and free MgS particles remain. MgS-free particles can inhibit the flow rate of the mixture because the MgS particles are in the form of fines.

3.4 Angle of Repose

The angle of repose test results are presented in Table 1 and Figure 6. A pharmaceutically good angle of repose for powders or powder mixtures is $\leq 40^\circ$ (Beakawi Al-Hashemi and Baghabra Al-Amoudi, 2018; Clayton, 2018; Zebua et al., 2023). In general, the mixture containing talc has the highest angle of repose (T0-T4). When forming a powder cone, the particles cannot move freely following the force of gravity because the particles below them restrain the movement of the particles above them. The powder cone becomes taller with a shorter base diameter. Irregular oval-shaped MCC particles dominate the mixture and have porosity so that the particle porosity becomes a stationary point holding the surrounding particles (Sheskey et al., 2017). The angle of repose improves along with increasing talc concentration (T0-T4). Talc particles can cover the porosity of MCC particles so that the MCC surface is flatter. This condition can reduce the stationary point holding particles, and the MCC

particles can quickly move. A similar angle of repose profile occurred in the mixture containing CA-LBG, but the value of the angle of repose was lower than the other two glidants. CA-LBG particles include esters, which can close the porosity of MCC particles and become slippery when rubbed against the surrounding particles. The initial angle of repose profile of the mixture containing MgS (M0-M2) is similar to the profile of the angle of repose of the other two glidants. Still, the value of the angle of repose is between the other two glidants. The lubrication mechanism also involves closing porosity and leveling the surface of the MCC particles. MgS particles are cohesive, requiring sufficient energy to interact with other particles (Goh et al., 2021; Peddapatla et al., 2016). This condition affects the strength of interaction with MCC particles and the quality of MCC particle movement in the powder. In experiment M4, the angle of repose increased again due to the excessive number of MgS particles in the mixture. MgS particles in the form of fines find it challenging to move and hold the particles around them.

3.5 Weight

Tablet weights for all experiments are presented in Table 1. Experiments were carried out to confirm that the mixture could flow and move to form tablets with the weight according to design. All mixtures can be compressed into tablets weighing about 700 mg with a narrow deviation. All mixtures can flow and move stably to fill the volume of the die chamber in the tablet compression machine.

3.6 Hardness

Tablet hardness test results are presented in Table 1 and Figure 7. Tablet hardness represents the interlocking strength between deformation particles of the tablet material. Each glidant produces varying tablet hardness because the glidant concentration influences it. The hardness profile of tablets containing talc shows high in experiments T0 and T1. Tablet hardness T0 (talc 0.5%) is controlled by the interlocking and deformation porosity of the MCC particles. The deformation of the talc particles fills the porosity of the deformation of the MCC particles so that the deformation arrangement of the particles is more stable and compact. Tablet hardness T1 (talc 1%) is similar in mechanism to T0, but the porosity between the deformation of MCC particles is full filled, more stable, and compact, so the tablet is more complex. The hardness of T2 and T4 is lower than T0 and T1 because the number of talc particles influences hardness. The large number of talc particles induces interlocking deformation of the talc particles when compressed. The interlocking formed is less strong because of the deformation of the talc particles in the form of fine particles (Sheskey et al., 2017). The tablet hardness graphic (M0-M4) in experiments containing MgS shows that the higher the MgS concentration, the lower the tablet hardness. MgS has a low bulk density (0.159 g/cm^3), so that a low concentration produces a large number of particles (Sheskey et al., 2017). The higher the MgS concentration, the more MgS particles will experience

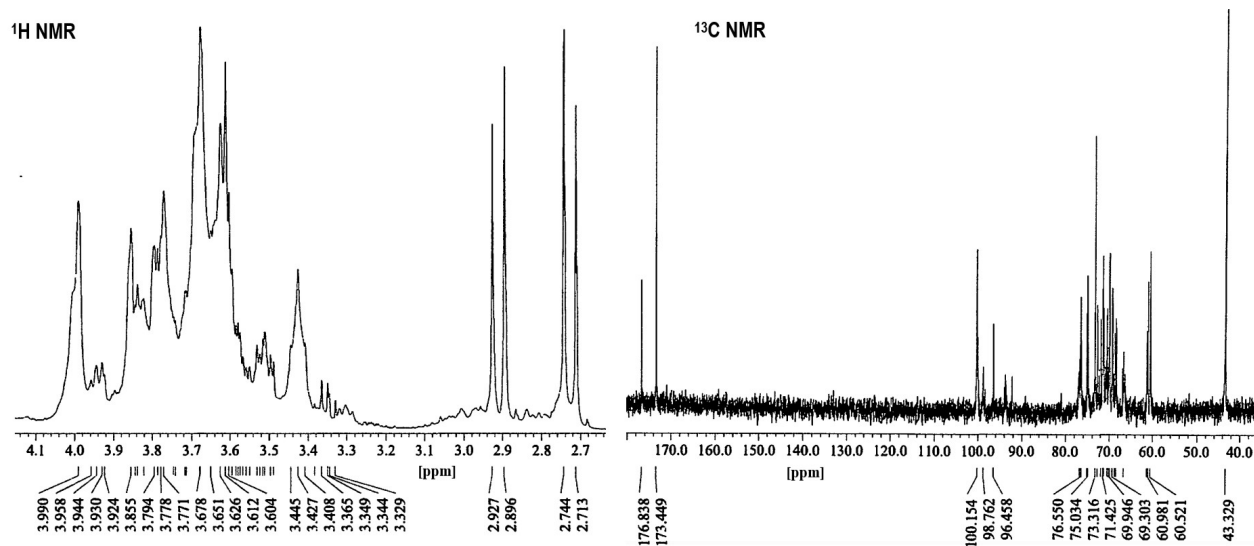


Figure 2. ^1H and ^{13}C NMR Spectra of CA-LBG

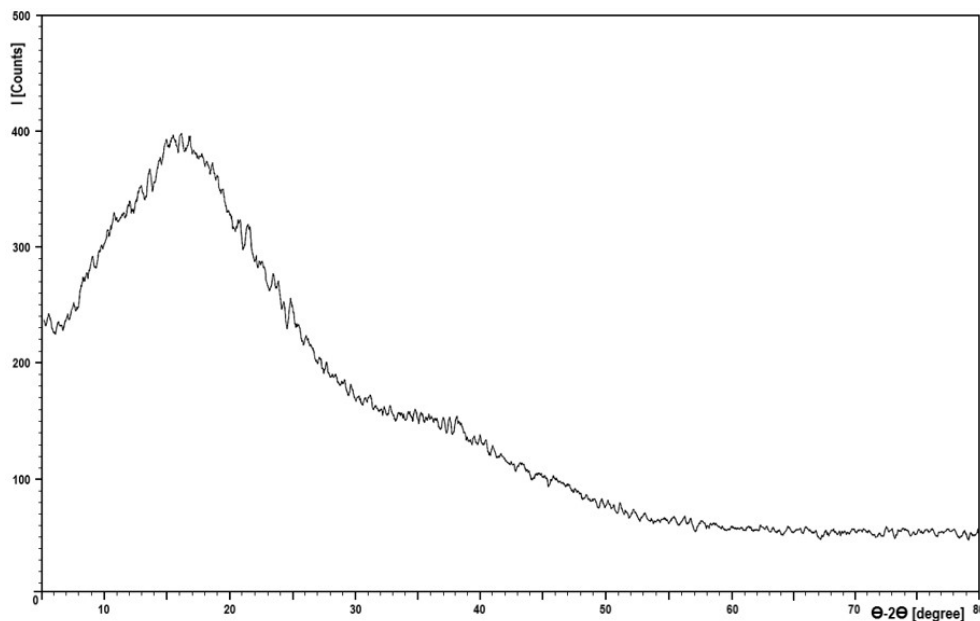


Figure 3. XRD Diffractogram of CA-LBG

interlocking deformation, and the higher the volume on dies in the tableting machine. The interlocking of low-density particles and fines results in weak tablet hardness. The hardness graph of CA-LBG tablets (C0-C4) contradicts MgS tablets. A high concentration of CA-LBG increases tablet hardness. When compressed, the fine and irregular particles of CA-LBG experience deformation and fill porosity of the deformation of the MCC particles. This condition causes the compactibility of the mixture to increase due to decreased porosity, making the resulting tablet hard. Besides that, CA-LBG is an ester derivative of LBG containing mannose and galactose. When compressed, mannose and galactose form a hard solid mass,

making the resulting tablet hard.

3.7 Friability

Tablet friability test results are presented in Table 1 and Figure 8. A pharmaceutically good friability for powders or powder mixtures is < 1% (Aslani and Beigi, 2016; Chee et al., 2017; Fouad et al., 2020; Osei-Yeboah and Sun, 2015). The friability profile of tablets containing MgS (M0-M4) shows that the higher the MgS concentration, the higher the friability. This condition is in line with the hardness profile of the tablet because the interlocking between deformation MgS particles is not strong, and the deformation MgS particles are easily

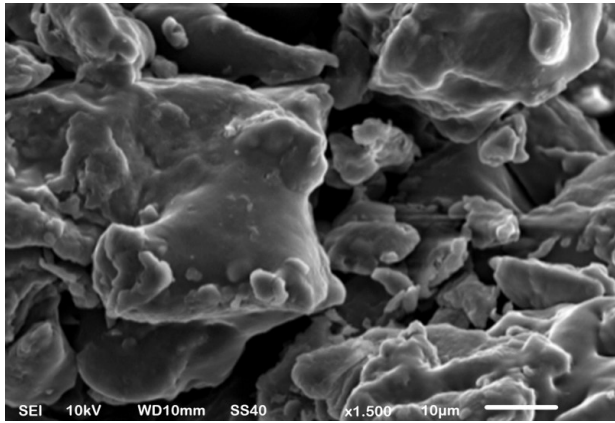


Figure 4. SEM Images of CA-LBG

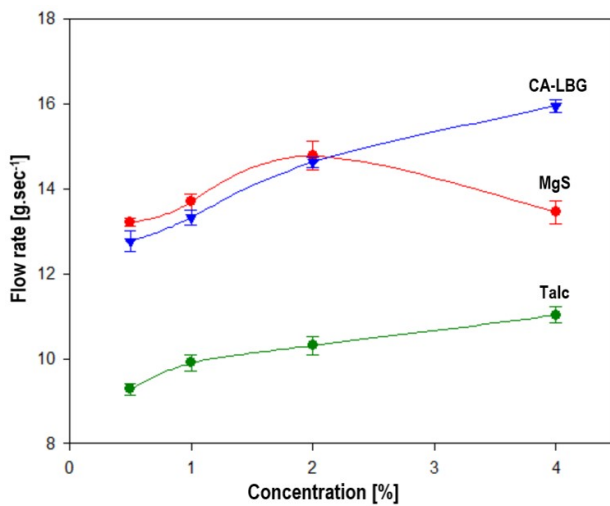


Figure 5. Profile of the relationship between glidant and the flow rate of the mixture. The ANOVA result of the type of glidant to flow rate is $F_{count} (1425.41) > F_{table} (3.40)$ and glidant concentration to flow rate is $F_{count} (139.52) > F_{table} (3.01)$, which means that the type of glidant and glidant concentration has an effect on the flow rate with a significance of 0.05.

separated. In addition, the fines of MgS tend to be on the tablet's surface so that the fines are easily separated when the tablet is rotated. Tablets containing CA-LBG showed increased friability at three initial concentrations (C0-C2). This condition is caused by the CA-LBG deformation not occupying the porosity between the MCC deformation. Fine particles from CA-LBG in small amounts choose to occupy the deformation surface of the MCC particles. In addition, the ester nature causes CA-LBG to tend to be hydrophobic, cohesive, and stick to the outer part of the tablet. Hence, the tablet is not strong and releases particles when there is mechanical movement. At high concentrations (C4), the porosity between MCC deformations is occupied by CA-LBG deformations due to their

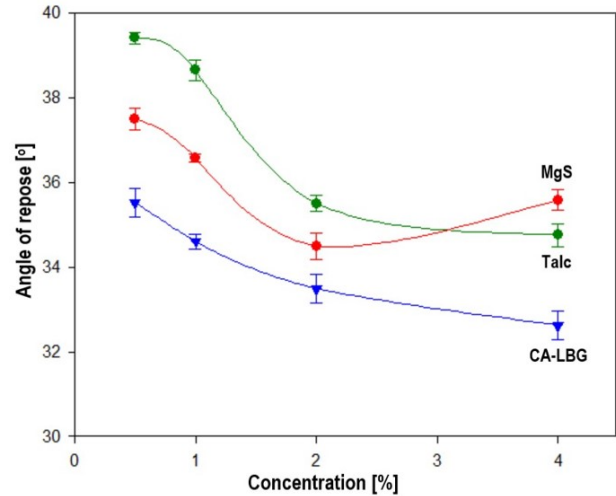


Figure 6. Profile of the relationship between glidant and the angle of repose of the mixture. The ANOVA result of the type of glidant to angle of repose is $F_{count} (424.27) > F_{table} (3.40)$ and glidant concentration to angle of repose is $F_{count} (331.92) > F_{table} (3.01)$, which means that the type of glidant and glidant concentration has an effect on the angle of repose with a significance of 0.05.

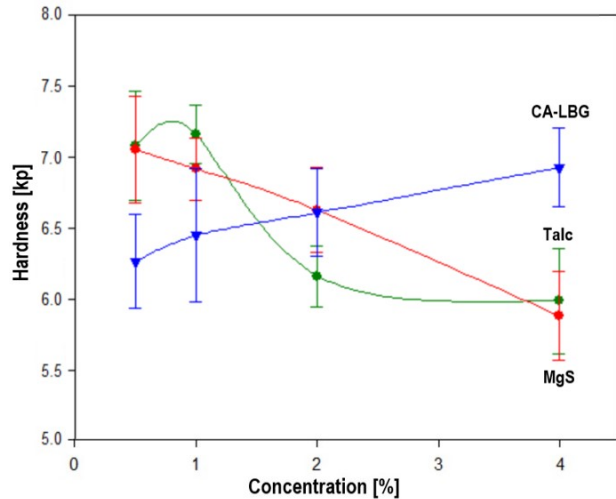


Figure 7. Profile of the relationship glidant and hardness. The ANOVA result of the type of glidant to the angle of repose is $F_{count} (0.52) < F_{table} (3.40)$ and glidant concentration to the hardness is $F_{count} (46.74) > F_{table} (3.01)$. The type of glidant has an effect that is not significant to the hardness, but glidant concentration has an effect on the hardness with a significance of 0.05.

excessive amount, so the tablet is more stable when rotated. The influence of the irregular shape of MCC after being compressed undergoes plastic deformation, causing the size of the porosity formed to vary. This porosity is filled by fine deformation of CA-LBG so that the tablet is stable when subjected

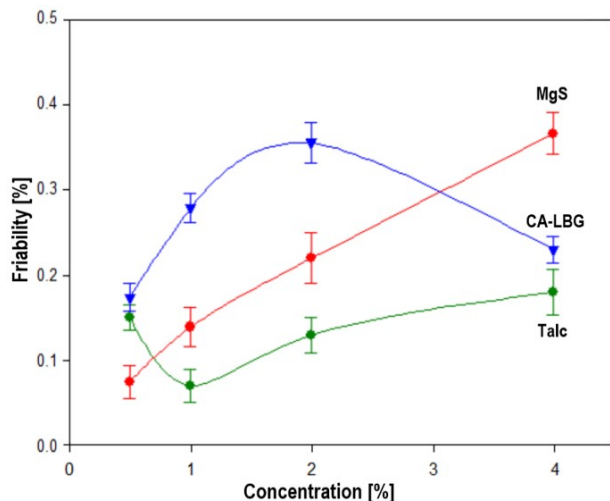


Figure 8. Profile of the relationship between glidant and tablet friability. The ANOVA result of the type of glidant to friability is $F_{count} (110.10) > F_{table} (3.40)$ and glidant concentration to friability is $F_{count} (69.34) > F_{table} (3.01)$, which means that the type of glidant and glidant concentration has an effect on the friability with a significance of 0.05.

to mechanical movement.

4. CONCLUSIONS

Based on experiments CA-LBG with compared talc and MgS as glidants, CA-LBG has potential as a glidant in MCC fillers. High concentration CA-LBG increases the mixture's flow rate, decreases the repose's angle, and hardens the tablet. CA-LBG concentrations of 0.5% and 4.0% in the mixture produced tablets with low friability.

5. ACKNOWLEDGMENT

The Author would like to thank the Ministry of Education, Culture, Research and Technology for research grant funding (0299/E3/2016), the Faculty of Pharmacy, Gadjah Mada University and the Faculty of Pharmacy, Widya Mandala Surabaya Catholic University for providing laboratory facilities. The Author also thanks Dr. Lannie Hadisoewignyo for donating several raw materials. The Author would like to thank Widya Mandala Surabaya Catholic University for subsidizing publication costs.

REFERENCES

Aslani, A. and M. Beigi (2016). Design, Formulation, and Physicochemical Evaluation of Montelukast Orally Disintegrating Tablet. *International Journal of Preventive Medicine*, **7**(1); 120

Aulton, M. E. and K. M. G. Taylor (2017). *Aulton's Pharmaceutics The Design and Manufacture of Medicines*, volume 5

Awad, A., S. J. Trenfield, and A. W. Basit (2020). Solid Oral Dosage Forms. In A. Adeboye, editor, *Remington The Science*

and Practice of Pharmacy. Elsevier Inc, 13th edition, pages 333–3358

- Beakawi Al-Hashemi, H. M. and O. S. Baghabra Al-Amoudi (2018). A Review on the Angle of Repose of Granular Materials. *Powder Technology*, **330**; 397–417
- Chee, T. L., F. A. A. Majid, and M. C. Iqbal (2017). Development of Diabecine™ Tablet and Confirmation of Its Physical Properties and Pharmaceutical Safety Analysis. *Sains Malaysiana*, **46**(4); 597–604
- Clayton, J. (2018). An Introduction to Powder Characterization. In *Handbook of Pharmaceutical Wet Granulation: Theory and Practice in a Quality by Design Paradigm*. Elsevier Inc
- Duan, P., B. Zhi, L. Coburn, C. L. Haynes, and K. Schmidt-Rohr (2020). A Molecular Fluorophore in Citric Acid/Ethylenediamine Carbon Dots Identified and Quantified by Multinuclear Solid-State Nuclear Magnetic Resonance. *Magnetic Resonance in Chemistry*, **58**(11); 1130–1138
- Fitrya, N. A. F. and B. U. A (2021). Tablet Formula Optimization From *Helminthostachys Zaylanica* Extract Using A SimplexLattice Design. *Science and Technology Indonesia*, **6**(3); 131–136
- Fouad, S. A., F. A. Malaak, M. A. El-Nabarawi, and K. A. Zeid (2020). Development of Orally Disintegrating Tablets Containing Solid Dispersion of a Poorly Soluble Drug for Enhanced Dissolution: In-Vitro Optimization/In-Vivo Evaluation. *PLoS ONE*, **15**(12 12); 1–17
- Gillet, S., M. Aguedo, C. Blecker, N. Jacquet, and A. Richel (2014). Use of ^{13}C -NMR in Structural Elucidation of Polysaccharides: Case of Locust Bean Gum. In *Young Belgium Magnetic Resonance Scientist 2014 (YBMRS 2014)*, volume 17
- Goh, W. P., A. M. Sanavia, and M. Ghadiri (2021). Effect of Mixer Type on Particle Coating by Magnesium Stearate for Friction and Adhesion Modification. *Pharmaceutics*, **13**(8); 1211
- Gustaman, F., K. Idacahyati, and W. T. Wulandari (2021). Formulation and Evaluation of Kirinyuh Leaf Effervescent Granules (*Chromolaena odorata*. L) as an Antioxidant. *Pharmacy Education*, **21**(2); 123–125
- Hadinugroho, W., K. Foe, Y. Tjahjono, C. Caroline, S. Yesery Esar, H. Wijaya, and M. Annabella Jessica (2022a). Tablet Formulation of 2-((3-(Chloromethyl)benzoyl)oxy)benzoic Acid by Linear and Quadratic Models. *ACS Omega*, **7**(38); 34045–34053
- Hadinugroho, W., S. Martodihardjo, A. Fudholi, and S. Riyanto (2017). Study of a Catalyst of Citric Acid Crosslinking on Locust Bean Gum. *Journal of Chemical Technology and Metallurgy*, **52**(6); 1086–1091
- Hadinugroho, W., S. Martodihardjo, A. Fudholi, and S. Riyanto (2019). Esterification of Citric Acid with Locust Bean Gum. *Heliyon*, **5**(8); e02337
- Hadinugroho, W., S. Martodihardjo, A. Fudholi, and S. Riyanto (2022b). Preparation of Citric Acid-Locust Bean Gum (CA-LBG) for the Disintegrating Agent of Tablet Dosage Forms. *Journal of Pharmaceutical Innovation*, **17**(4);

- 1160–1175
- Hadinugroho, W., S. Martodihardjo, A. Fudholi, S. Riyanto, and J. Prasetyo (2023). Hydroxypropyl Methylcellulose as Hydrogel Matrix and Citric Acid-Locust Bean Gum as Negative Matrix for Controlled Release Tablet. *ACS Omega*, **8**(8); 7767–7778
- Idström, A., S. Schantz, J. Sundberg, B. F. Chmelka, P. Gatenholm, and L. Nordstierna (2016). ¹³C NMR Assignments of Regenerated Cellulose from Solid-State 2D NMR Spectroscopy. *Carbohydrate Polymers*, **151**; 480–487
- Isasi, M. P. and J. Ramón (2022). and Biopharmaceutical Applications. *Molecules*, **22**; 8265–8281
- Jayani, N. I. E., B. L. Salawane, H. Y. Pelopolin, and K. C. Rani (2021). Formulation and Evaluation of Two Types of Functional Beverage Granules Made of Extracts of Guava Leaves, Purple Sweet Potato and Cinnamon. *Tropical Journal of Natural Product Research*, **5**(6); 1024–1029
- Kim, J. Y., Y. K. Lee, and Y. H. Chang (2017). Structure and Digestibility Properties of Resistant Rice Starch Cross-Linked with Citric Acid. *International Journal of Food Properties*, **20**(2); 2166–2177
- Krivokapić, J., J. Ivanović, J. Djuriš, D. Medarević, Z. Potpara, Z. Maksimović, and S. Ibrić (2020). Tableting Properties of Microcrystalline Cellulose Obtained from Wheat Straw Measured with a Single Punch Bench Top Tablet Press. *Saudi Pharmaceutical Journal*, **28**(6); 710–718
- Luh Putu Wrasati, M. D. W. and I. N. K. Putra (2021). Characteristics of Effervescent Granules Extract of Kenikir (*Cosmos caudatus* Kunth) Leaf with Various Acid Compositions as Alternative Functional Beverage Products. *International Journal of Current Microbiology and Applied Sciences*, **10**(8); 1–8
- Meng, Y., W. Xie, H. Wu, S. M. Tariq, and H. Yang (2022). Evolution of Black Talc upon Thermal Treatment. *Minerals*, **12**(2); 1–14
- Osei-Yeboah, F. and C. C. Sun (2015). Validation and Applications of an Expedited Tablet Friability Method. *International Journal of Pharmaceutics*, **484**(1–2); 146–155
- Peddapatla, R. V. G., C. A. Blackshields, M. F. Cronin, and A. M. Crean (2016). Behaviour of Magnesium Stearate in Continuous Feeding. *Food, Pharmaceutical and Bioengineering Division 2016 - Core Programming Area at the 2016 AIChE Annual Meeting*, **1**; 515–518
- Pratiwi, M., P. Ylittervo, A. Pettersson, T. Prakoso, and T. H. Soerawidjaja (2017). Magnesium Stearine Production via Direct Reaction of Palm Stearine and Magnesium Hydroxide. *IOP Conference Series: Materials Science and Engineering*, **206**(1); 012026
- Putri, N. S. F. (2023). The The Effect Of Uncontrolled Addition Of Gelatin In Paracetamol Tablet Formulation And The Evaluation. *Journal of Science and Technology Research for Pharmacy*, **2**(1); 31–37
- Sheskey, P. J., C. G. Walter, and C. G. Cable (2017). *Handbook of Pharmaceutical Excipients*. Pharmaceutical Press and American Pharmacists Association, 8th edition
- Singh, R. S., N. Kaur, V. Rana, R. K. Singla, N. Kang, G. Kaur, H. Kaur, and J. F. Kennedy (2020). Carbamoyl ethyl Locust Bean Gum: Synthesis, Characterization and Evaluation of Its Film Forming Potential. *International Journal of Biological Macromolecules*, **149**; 348–358
- The United States Pharmacopeial Convention (2018). *Pharmacopeia 41-National Formulary 36. 5*. Vol. 5, Issue 1
- Tian, D., Y. Qiao, Q. Peng, Y. Zhang, Y. Gong, L. Shi, X. Xiong, M. He, X. Xu, and B. Shi (2023). A Poly-D-Mannose Synthesized by a One-Pot Method Exhibits Anti-Biofilm, Antioxidant, and Anti-Inflammatory Properties In Vitro. *Antioxidants*, **12**(8); 1–21
- Tikhonov, I. V., V. V. Sokolov, V. M. Shchetinin, T. E. Chernykh, A. Y. Kutyurin, and D. A. Bakulin (2019). Supramolecular Structure of Rugar-S and Rugar-NT Aramid Fibers. *Fibre Chemistry*, **51**(2); 101–104
- Trabelsi, I., S. Ben Slima, N. Ktari, M. Bouaziz, and R. Ben Salah (2021). Structure Analysis and Antioxidant Activity of a Novel Polysaccharide from Katan Seeds. *BioMed Research International*, **2021**; 1–13
- Zarmpi, P., T. Flanagan, E. Meehan, J. Mann, and N. Fotaki (2020). Impact of Magnesium Stearate Presence and Variability on Drug Apparent Solubility Based on Drug Physicochemical Properties. *AAPS Journal*, **22**(4); 1–18
- Zebua, N. F., T. Alexandro, V. W. Pratiwi, S. Nadia, S. Hidayat, M. Fujiko, M. Saputri, T. K. Bakri, and Nerdy (2023). Tablet Formulation with Galactomannan Binding Agent and Acute Toxicity Test from *Terminalia catappa* L. *Science and Technology Indonesia*, **8**(1); 129–136
- Zhang, Y. l., C. x. Zhao, X. d. Liu, W. Li, J. l. Wang, and Z. g. Hu (2016). Application of Poly(aspartic acid-citric acid) Copolymer Compound Inhibitor as an Effective and Environmental Agent Against Calcium Phosphate in Cooling Water Systems. *Journal of Applied Research and Technology*, **14**(6); 425–433
- Zheng, X. X., Y. C. Pan, and W. F. Sun (2022). Water-Tree Characteristics and Its Mechanical Mechanism of Crosslinked Polyethylene Grafted with Polar-Group Molecules. *International Journal of Molecular Sciences*, **23**(16); 9450